Computational Study of the Citrate Synthase Catalyzed Deprotonation of Acetyl-Coenzyme A and Fluoroacetyl-Coenzyme A: Demonstration of a Layered Quantum Mechanical Approach

Wei Yang and Dale G. Drueckhammer*

Department of Chemistry, State University of New York at Stony Brook, Stony Brook, New York 11794-3400

Received: March 19, 2003

The reaction of the enzyme citrate synthase was studied using the ONIOM method, in which different layers of the system are evaluated using different levels of quantum mechanical theory. A 10 Å radius model of the citrate synthase active site and surrounding protein environment was studied using MOZYME as the low level to describe the larger portion of the system. MOZYME is a semiempirical method in which the computational time scales linearly with the size of the system, enabling quantum mechanical calculations on fairly large molecular systems. Higher level ab initio methods were used to evaluate the reactive portion of the substrate and active site functionality directly involved in the reaction. This novel ONIOM−MOZYME method produced results that agree with previous studies that predict an enolate intermediate in the citrate synthase catalyzed deprotonation of acetyl-coenzyme A (acetyl-CoA). The calculated activation energy for enolate formation (14.8 kcal/mol) is very close to the experimentally determined free energy of activation. Calculated energies for an enol intermediate or a half-protonated enolic intermediate stabilized by a low-barrier hydrogen bond are 10−13 kcal/mol higher. The ONIOM−MOZYME method was also used to study the citrate synthase catalyzed deprotonation of fluoroacetyl-CoA. The results rationalize the stereoselectivity observed in the deprotonation of fluoroacetyl-CoA in the context of an enolate intermediate. This provides a reconciliation of the stereoselectivity in deprotonation of fluoroacetyl-CoA, which was previously attributed to an enol intermediate, with other studies that support an enolate intermediate for the reaction of citrate synthase. The ONIOM−MOZYME method is demonstrated to be a powerful method for the prediction of mechanism and activation energy and for analysis of structural changes in the active site during catalysis.

Introduction

The deprotonation of a weakly acidic carbon acid is a common enzyme-catalyzed reaction, typically involving a C−H bond activated by a neighboring carbonyl group.[1] This transformation is somewhat remarkable considering that the inherent difference in acidity between the substrate and the conjugate acid of a typical active-site base is on the order of 13−15 pK_a units.[2] An important aspect of understanding how an enzyme can overcome this considerable thermodynamic barrier is knowing the nature of the intermediate involved. Both enol and enolate intermediates have been proposed for these reactions, as well as an "enolic" intermediate stabilized by a low-barrier or short, strong hydrogen bond (Scheme 1). Stabilization of the intermediate is thus achieved through proton donation or electrostatic charge stabilization or both.[2−5]

The nature of the intermediate in the deprotonation of acetyl-coenzyme A by the enzyme citrate synthase (Scheme 1) has been the subject of extensive computational studies.[6−10] The relative energies of the three possible intermediates have been evaluated using several computational techniques including semiempirical (AM1) treatment of a small active site model,[6] as well as QM/MM (AM1/CHARMM, MP2/6-31G(d)/CHARMM//HF/6-31G(d)/CHARMM)[7,9] and QM-FE (MP2/6-31+G*//HF/6-31+G*:AMBER free energy)[10] methods that consider the greater protein environment. The stationary structures (reactant, transition state, and product) treated by previous quantum mechanical calculations are optimized with limited inclusion of the enzymatic environment, considering Asp375, His274, and the thioacetate portion of acetyl-CoA only.[7,10] This may not well represent the enzymatic environment, which provides additional conformational constraints and electrostatic interactions, though it can provide valuable initial information for the model reaction. The corresponding structures obtained from QM/MM calculations[7,9] were obtained with consideration of the enzymatic environment, which was treated by a classical

SCHEME 1: The Reaction of Citrate Synthase with Three Possible Intermediates

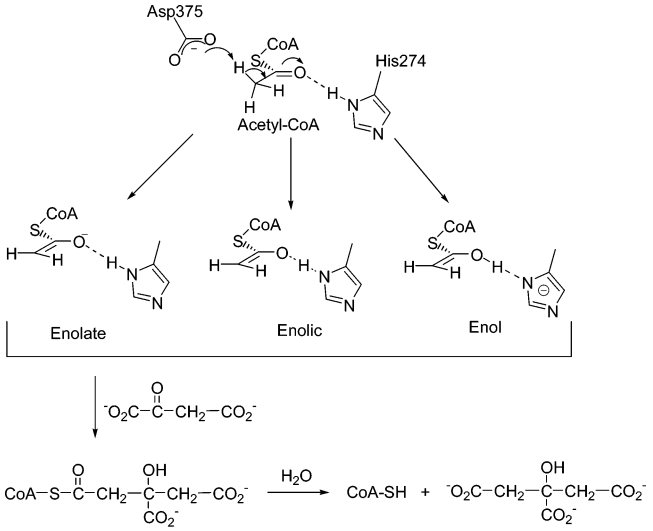

10.1021/jp034717v CCC: $25.00
Published on Web 05/24/2003

force field. Though there is some disagreement among these calculations,[10] they consistently predict that an enolate is the true intermediate. In the citrate synthase catalyzed reaction of the unnatural substrate fluoroacetyl-CoA, the pro-S proton of fluoroacetyl-CoA is removed with very high selectivity ($\Delta\Delta G$ > 3 kcal/mol).[11,12] Analysis of the crystal structure of citrate synthase and its substrate analogue complexes indicates that the E isomer of the intermediate is thus formed.[13,14] Quantum mechanical calculations based on a simple model of the intermediate indicated that the E enol is more stable than the Z enol by 4.3 kcal/mol, while the isomeric enolates differ in energy by only 1.1−1.9 kcal/mol.[15,16] An enol intermediate was thus proposed to explain the high selectivity in the deprotonation of fluoroacetyl-CoA.

Models for several enzymatic reactions incorporating the portion of the substrate and active site functionality directly involved in the reaction have been studied by quantum mechanical calculations.[17−19] Such models have sometimes been called theozymes or compuzymes.[20] Because of the time-consuming nature of quantum mechanical calculations, a limited number of atoms from the enzyme can be included in the model, and this may not accurately describe the enzymatic environment. The recently developed method MOZYME, based on the common semiempirical method PM3, allows quantum calculations on much larger systems.[21−23] MOZYME uses localized molecular orbitals to solve the neglect of diatomic differential overlap (NDDO) self-consistent field equation, in contrast to conventional molecular orbitals, which extend over all atoms. With localized molecular orbitals, the computational time scales linearly with the number of atoms in the system, whereas with conventional semiempirical methods, the computational time is approximately proportional to the number of orbitals to the third power. MOZYME calculations on molecular systems of up to several thousand atoms are thus possible, and this method has even been used to study enzymatic reactions.[21,22] However, semiempirical methods have limited accuracy in describing transition states and reaction pathways.

While previous work has shown that accurate computational description of the citrate synthase reaction requires high-level quantum calculations, evaluation of the citrate synthase catalyzed reaction of fluoroacetyl-CoA requires consideration of all of the active site functionality that interacts with the fluorine atom or the environment of which is affected by the presence of the fluorine atom. Understanding the charge transfer and polarization effects of the protein on the reaction requires electronic structural treatment of the enzymatic environment. This paper describes studies of the citrate synthase catalyzed reactions of acetyl-CoA and fluoroacetyl-CoA using the hybrid methodology ONIOM, which treats the system as layers and performs different level quantum mechanical calculations on each layer.[24−27] The ONIOM method has previously been used to study complex organic reaction systems such as organometallic reactions and has recently been applied to models of enzymatic reactions.[17,24−27] In the work described here, the reaction center of citrate synthase is treated with high-level ab initio and density functional calculations, while a 10 Å radius surrounding area of the enzyme active site is treated using MOZYME. The deprotonation of acetyl-CoA is reevaluated using this method, and the issue of stereoselectivity in the deprotonation of fluoroacetyl-CoA is addressed. The results further support an enolate intermediate in the reaction of citrate synthase and reconcile the stereoselectivity in the deprotonation of fluoroacetyl-CoA with an enolate. This work demonstrates that the combination of ONIOM and MOZYME permits the study of an enzymatic reaction model including several hundred atoms.

Computational Details

Modeling Tools. All ab initio and density functional calculations were performed with Gaussian 98.[28] Calculations involving MOZYME were performed with MOPAC 2000.[29] Molecular dynamics calculations were performed with the Discover module of Insight II (Accelrys).

System Preparation. The crystal structure of the complex of citrate synthase with the acetyl-CoA analogue amidomethyldethia-CoA (AMX), in which the acetylthio moiety of acetyl-CoA is substituted by an amidomethylene group (1csh, 1.6 Å, from chicken heart) was chosen to generate the initial model for this study (numbering is based on the pig heart enzyme).[13] Protons were introduced through Insight II Builder (Accelrys) by setting the charge of residues according to their pK_a values, and histidine residues were set up as neutral (tauomer states NE or ND were designated according to local hydrogen-bonding environments and were later confirmed in the molecular dynamics (MD) relaxed structure). A modified structure in which AMX was replaced with acetyl-CoA was put in a box of water of dimensions 43 × 33 × 30 Å^3 to fill the cavity around the reaction center. Molecular dynamics calculations were performed on the entire citrate synthase dimer to relax the strain in the crystal structure with added water molecules. No boundary or periodic condition was applied. The Amber force field (AMBER95)[30] was used with the addition of parameters for the torsional terms for the thioester moiety of acetyl-CoA and stretching, angle, and torsional terms for oxaloacetate and the fluorothioester moiety of fluoroacetyl-CoA obtained by fitting Merck molecular force field (MMFF)[31] calculations using Spartan.[32] The charges for acetyl-CoA and fluoroacetyl-CoA were generated by the restrained electrostatic potential (RESP) method.[33] A 12 Å nonbonded cutoff was used in molecular dynamics simulations. Restrained molecular dynamics simulation was run at 300 K with backbone heavy atoms of the protein and the 3′-phospho-ADP portion of CoA fixed, and equilibrium was reached after about 200 ps, monitored by potential energy, total energy, and temperature. The enzyme complexes with fluoroacetyl-CoA and with the enolates of acetyl-CoA and fluoroacetyl-CoA were constructed by modification of the acetyl group of the acetyl-CoA complex. Short molecular dynamics simulations were performed for relaxation of the fluoroacetate and enolate moieties with the remainder of the structure fixed. From each of these refined structures, a supercluster was defined by a sphere of 17 Å radius around the reaction center carbon atom with residues at the interface included in the cluster. Each of these clusters underwent restrained energy minimization using MOZYME with positions of heavy atoms of the protein and substrate or intermediate outside the cluster being frozen. Eigenfollowing energy minimization convergence criteria was set up with 0.002 trust radius. The minimized structure was close to the crystal structure with 0.85 Å root-mean-square deviation (rmsd) for heavy atoms. By the same procedure, a cluster with 10 Å radius (large model, Figure 1) was selected, removed from the outer structure, and minimized using MOZYME by restraining all heavy atoms of the protein backbone. The large model included His235, His238, Asn242, Val243, Ser244, Leu269, Pro272, Leu273, His274, Gly275, Leu276, Ala277, Asn278, Gly317, Tyr318, Gly319, His320, Ala321, Leu323, Arg329, Asn373, Val374, Asp375, Ala376, Phe397, and Arg401. This model appears to include all residues that could have a direct effect on the energy barrier during the deprotonation of acetyl-

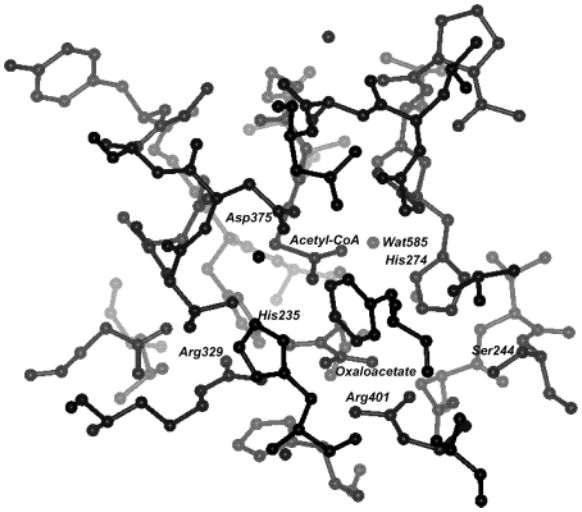

Figure 1. The 10 Å radius large model.

CoA. The N-terminal nitrogen in the large model was made a neutral amine, and the C-terminus was made an aldehyde. The large model contained four water molecules from the crystal structure and an additional two water molecules originating from the molecular dynamics simulation. The rmsd for heavy atoms relative to the crystal structure was 0.6 Å.

Reaction Pathway Generation. From the refined 10 Å radius large models, smaller medium-size models were defined by manual selection of atoms of the substrate and enzyme side chains that directly interact with the reactants (Figure 2). The model so defined for the complex of acetyl-CoA and its enolate consisted of 143 atoms. The corresponding medium-size model for fluoroacetyl-CoA and its enolate consisted of 232 atoms to include additional amino acid side chains positioned to interact with the fluorine atom.

Two-layer ONIOM (HF/6-31+G*, PM3) was used to optimize the structures of the medium-size models.[24−27] The small model of the reaction center calculated at the higher level consists of the (fluoro)acetylthiomethylene portions of acetyl-CoA or fluoroacetyl-CoA, Wat585, and the side chains of Asp375 and His274 (Figure 3). Hydrogen atoms were substituted for bonds to atoms of the medium-size model layer in high-level calculations of the small model. Positions of backbone atoms of the protein and of atoms of acetyl-CoA beyond the amide bond nearest the thioester were frozen. On the basis of the enzyme−substrate and enzyme−enolate complex models thus generated, the QST2 procedure was used to locate and optimize the transition-state structures for formation of the enolates of acetyl-CoA and fluoroacetyl-CoA.[34] Intrinsic reaction coordinate (IRC) calculations were performed to verify transition-state structures. Normal-mode analyses were performed in the small model scaled by 0.93 in the HF/6-31+G* level. To characterize the proposed enolic and enol intermediates, a pseudo-proton-transfer process was modeled by coordinate driving involving proton transfer from His274 nitrogen to the acetyl-CoA enolate oxygen. A total of 18 points were used for following the proton-transfer pathway with steps of 0.05 Å. The same result was obtained when the proton transfer was conducted in the reverse direction.

TABLE 1: Energy Changes upon Active Site Deletions Calculated at the B3LYP/6-31+G* Level

species deleted	ΔE(transition state), kcal/mol	ΔE(enolate complex), kcal/mol
oxaloacetate	−7.2	−17.0
Wat596	−2.6	−5.6
Wat584 and Wat586	2.3	4.0
Ser244 → Gly	0.3	1.0
His235 → Gly	4.1	5.9
Wat585	6.1	9.7
Wat585 + His235 → Gly	8.7	14.5

The atomic positions in these optimized medium-size models were then substituted for the corresponding atoms in the large models. With the positions of the medium-size model atoms frozen, the large models were optimized individually by MOZYME while keeping the atoms outside the large model sphere frozen in positions defined in the initial system preparation procedure.

Energy Calculations. Final energy was calculated, according to the energy expression of two-layer ONIOM:

$$E(\text{ONIOM2}) = E(\text{High, SModel}) + E(\text{Low, LModel}) - E(\text{Low, SModel})$$
$$= E(\text{High, SModel}) + \Delta E(\text{Low, LModel} \leftarrow \text{SModel})$$

where High and Low refer to high- and low-level calculations and SModel and LModel refer to the central reaction core treated at the high level and to the 10 Å radius large model, respectively.[24] HF/6-31+G* was used as the high calculation level, and MOZYME was used as the low level. Single-point energies for the HF-derived high-level layer were also calculated using MP2/6-31+G* and B3LYP/6-31+G*. Zero-point energy correction was performed at the HF/6-31+G* level for all energy calculations.

Component Analysis and NBO Analysis. For analysis of the role of individual substrate and amino acid side chain functionality, ground state, transition state, and enolate complex energies were calculated at the B3LYP/6-31+G* level with omission of selected functionality from the model. Structures of the deletion complexes were not further optimized. Comparison to calculated energies for the original model was used to calculate energy changes resulting from the deletions (Table 1). NBO natural population analysis was performed at the B3LYP/6-31+G* level.

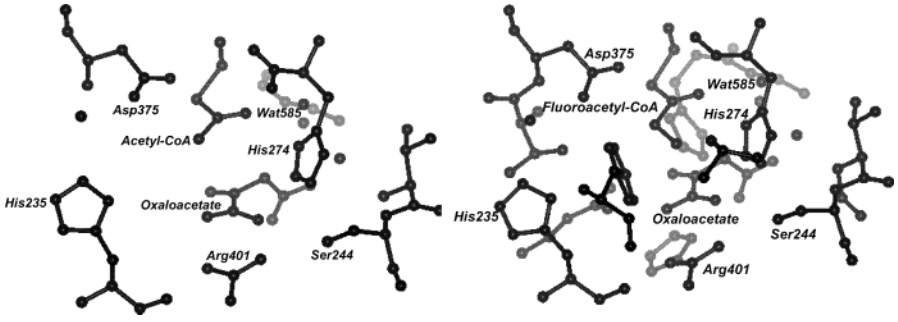

Figure 2. The medium-size models used for reaction pathway generation: (left) for acetyl-CoA; (right) for fluoroacetyl-CoA.

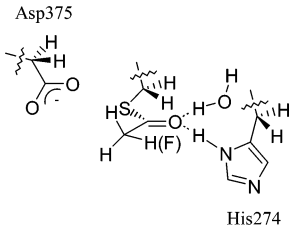

Figure 3. The small model treated by quantum mechanical methods in ONIOM calculations.

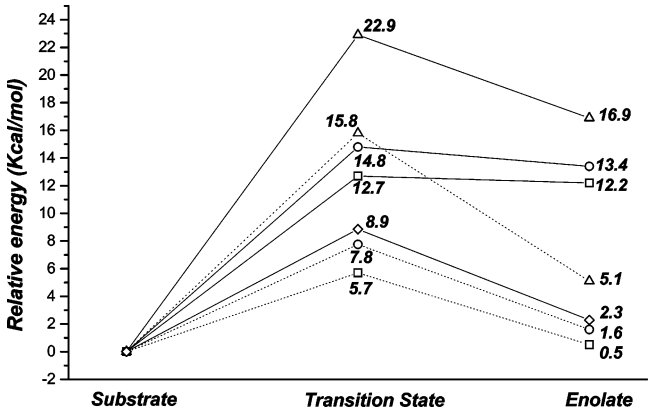

Figure 4. The energy profile for formation of the acetyl-CoA enolate complex with energy of the acetyl-CoA complex as standard. (◊) MOZYME; (△) HF/6-31+G*; (○) MP2/6-31+G*; (○) B3LYP/6-31+G* (MP2 and B3LYP values are single-point energies based on the HF-derived geometry); (dotted line) for the small model only, including zero-point energy correction at the HF/6-31+G* level; (solid line) for the large model calculated using ONIOM−MOZYME.

Results and Discussion

A multilayer model of citrate synthase was employed in this work. The model was constructed from the crystal structure of the complex of citrate synthase with the potent acetyl-CoA analogue inhibitor amidomethyldethia-CoA (AMX). This structure provided the tightest and highest-resolution structural model for the complex of citrate synthase with acetyl-CoA and with potential reaction intermediates. A 17 Å radius sphere (supercluster) of the protein surrounding the active site served as an interface between quantum mechanically treated inner layers and the molecular mechanics optimized outer enzyme structure in developing the model. Inside this supercluster, a 10 Å radius sphere was defined as the large model (Figure 1). This represents the region treated using MOZYME in two-layer ONIOM calculations. The medium-size model contains only the reactants and amino acid side chains positioned to interact directly with the reactants (Figure 2). This medium-size model was optimized by ONIOM using semiempirical (PM3) calculations as the low level in generation of the reaction pathway and in evaluation of possible enolic and enol intermediates. The small model contains only the portion of the reactants and amino acid side chains directly involved in the reaction and is the region treated by high-level quantum methods in two-layer ONIOM calculations (Figure 3).

Formation of the Enolate from Acetyl-CoA. Figure 4 shows the energy results for formation of the enolate from acetyl-CoA. The dotted lines indicate the energetics of the small model only, while the solid lines correspond to the energy of the entire large model. While the activation energies calculated at the MP2 and B3LYP levels are in close agreement, the activation energy calculated at the HF level is much higher, suggesting a large electron correlation effect. In this and previous studies, MP2 calculations give an activation energy slightly lower than the experimentally determined value of 14.7 kcal/mol, though the experimental number is the free energy of activation.[7,9] The B3LYP calculations reproduce the experimental value very well. When the entire large model was treated simply using MOZYME, a much lower-energy barrier of 8.9 kcal/mol was obtained. This may reflect the limitations of semiempirical calculations in dealing with transition states and demonstrates the advantage of high-level calculations in the reaction center using ONIOM. The ONIOM/MOZYME study indicates that the transition state leading to the enolate has only slightly higher energy than the enolate itself, as also observed in the QM/MM calculations of Mullholland et al. and as assumed in the QM-FE study of Donini et al.[6,7,10] In contrast, the enolate has substantially lower energy than the transition state in the small model layer of ONIOM alone.

The calculated energy barrier and the energy of the enolate relative to substrate are both substantially lower in the small model alone relative to the overall energies of the large model. This was also observed in previous QM/MM studies, though QM-FE calculations show higher energy in the absence of the enzyme environment.[9,10] This difference may be related to the fact that in both the present ONIOM/MOZYME study and the previously reported QM/MM study simultaneous geometry optimization of the small and larger models were performed while in the QM-FE study the constrained small model was fit into into the enzyme. In the QM-FE study,[10] the enthalpy of activation was calculated for the QM component (His374, Asp375, and thioacetate), while free energy was calculated only for the MM and QM/MM interaction components. Thus some comparison of the energy barrier from the current work with that of the QM-FE study may be valid for the small model. However, the free energy from the MM and QM/MM interaction components may buffer the larger enthalpy barrier from the QM component computed by a constrained small model without the enzymatic environment, thus effecting comparison with the results of this study.

Figure 5 shows structures in the pathway for enolate formation, while Figure 6 gives interatomic distances and atomic charges derived from NBO analysis for the small model. The reaction center structures derived from this work are more similar to the structures from QM/MM calculations than to those from the QM-FE studies. For example, His274 forms a shorter hydrogen bond to the hydroxyl group of Ser244 (3.00 Å) than to the backbone N−H (3.45 Å), as in the QM/MM studies.[9] The negative charge on the carboxylate oxygens of Asp375 is shown to decrease by 0.15 and 0.27 in the transition state and enolate complex, respectively, while positive charge on the proton being transferred increases by 0.14 and 0.21 units. The changes in charge on the carboxylate oxygen atoms are similar to those in a simple model for citrate synthase consisting only of a carboxylate group representing the side chain of Asp 375 and the acetyl thioester moiety in the absence of any additional enolate-stabilizing groups, though the charges were calculated differently.[6] In this previous model, the change in charge on the transferred proton is more fully observed in the transition state.[6] For the acetyl thioester, positive charge character on the methyl carbon decreases by 0.14 in the transition state but comes back to near that of the substrate in the enolate complex. In contrast, changes in charge of the carbonyl carbon and carbonyl oxygen are very small in the transition state but are substantial in the enolate complex (−0.18 and −0.17, respectively). This is consistent with little resonance delocalization of charge in the transition state but more substantial delocalization in the enolate. Changes in bond lengths mirror the charge effects,

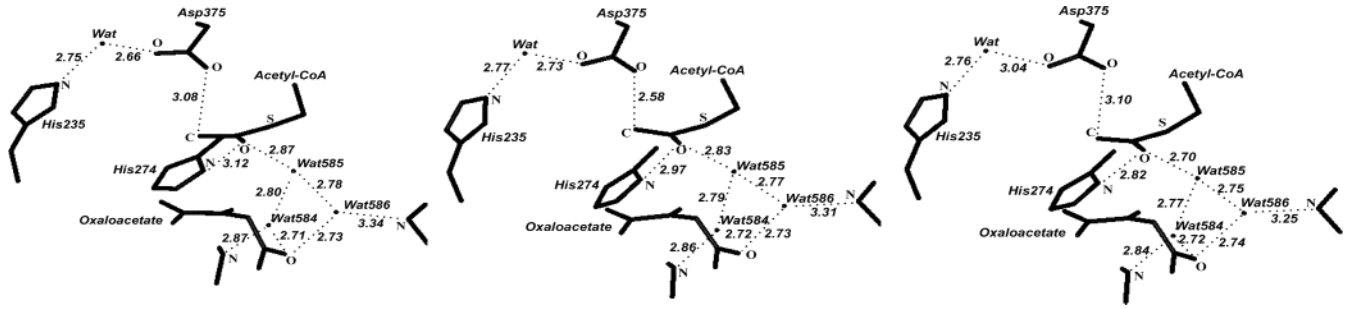

Figure 5. Structures in the reaction pathway for formation of the acetyl-CoA enolate: (left) reactant; (middle) transition state; (right) enolate.

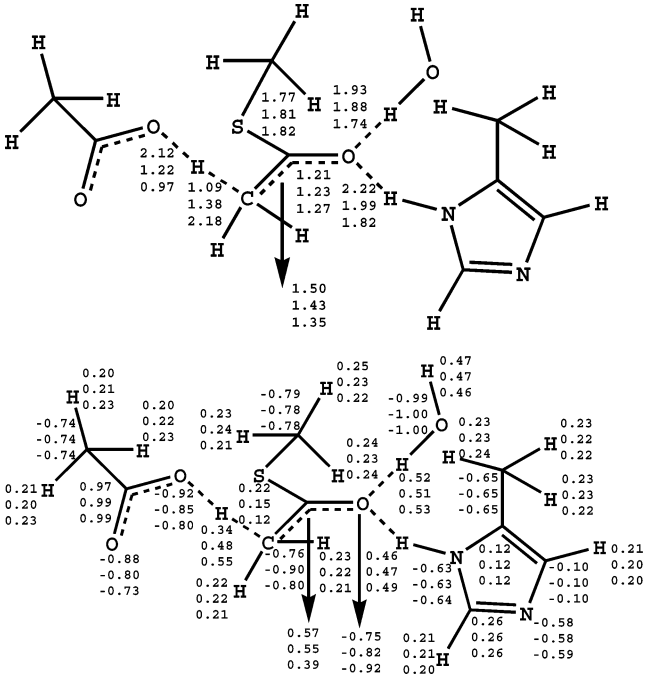

Figure 6. Values for interatomic distances (upper) and atomic charges (lower) determined by NBO analysis for the substrate (upper values), transition state (middle values), and enolate (lower values) complexes.

showing shortening of the C−C bond and lengthening of the C═O bond by small amounts in the transition state and by larger amounts in the enolate. In the previous simple model, the charges and bond distances in the transition state are much nearer to those of the enolate.[6] Atomic charges also indicate some charge stabilization of the enolate by the sulfur atom, as has been observed in the previous citrate synthase model and in a recently reported model for enolate formation by acyl-CoA dehydrogenase.[6,35] Bond distances show a decrease in the Asp375 oxygen to methyl carbon distance from 3.08 Å in the ground state to 2.58 Å in the transition state and lengthening to 3.10 Å in the enolate complex. This is consistent with the strongest bonding between Asp375 and the acetyl-CoA methyl group in the transition state, as also observed in previous computational models.[6,35] Hydrogen bonds to the carbonyl oxygen also shorten substantially in the transition state and enolate complexes, as observed in the previous studies.[6,35]

The ONIOM−MOZYME-derived structures show the substrate complex to be more similar to the transition state and enolate complexes, relative to structures from QM-FE studies and in the small model used in QM/MM calculations.[7,10] This point is observed in comparing relative atomic charges in the three complexes and may indicate greater polarization of the acetyl group of the substrate complex toward the transition state for enolate formation in the ONIOM−MOZYME calculations. The structures of the reaction center are more compact relative to the QM-FE structure and the QM/MM small model, which may be enforced by the enzymatic environment despite some simple constraints to mimic the enzymatic environment in the QM-FE calculations. The enforced positioning of catalytic groups relative to the substrate has analogy to the near attack conformer strategy proposed for enzymatic nucleophilic substitution reactions.[36] Generation of the reaction center separately from the enzymatic environment may fail to duplicate these important effects in enzyme catalysis. The structures from QM/MM calculations are more similar than the QM-FE structures to the structures from this study. The small overall activation energy difference between ONIOM−MOZYME (14.7 kcal/mol) and QM/MM (17.9 kcal/mol) studies may be due to the more extensive inclusion of quantum effects such as charge transfer and polarization in the ONIOM−MOZYME calculations.

It was proposed that an unfavorable interaction between the dianionic electrophilic substrate oxaloacetate and the enolate may be responsible for increasing the energy barrier in the larger enzyme environment.[9,10] Active site deletions were studied at the B3LYP/6-31+G* level to evaluate the impact of oxaloacetate and nearby water molecules and amino acid side chains on the stability of the enolate complex and on the transition state for its formation (Table 1). The results indicate that oxaloacetate indeed has a very large destabilizing effect on the enolate complex and a somewhat smaller though still substantial effect in the transition state. Wat596 also has a substantial destabilizing effect on the enolate and transition-state complexes relative to the substrate complex. This apparently results from stabilization of the carboxylate of Asp375 by Wat596 in the substrate complex. The naked carboxylate of the small model is highly basic and not representative of the hydrogen-bonded environment of the Asp375 carboxylate in the active site of citrate synthase. A related view is that during the reaction, the hydrogen-bonding network between Asp375 and His235 bridged by Wat596 becomes weaker as the enolate is formed and Asp375 becomes protonated (Figure 5). Water molecules 584, 585, and 586 and the side chains of Ser244 and His235 all have stabilizing effects on the transition state for enolate formation. Wat585 directly stabilizes the enolate by hydrogen-bond donation to the enolate oxygen. Water molecules 584 and 586 both form hydrogen bonds to Wat585 and to the carboxylate oxygen of oxaloacetate.[7] His235 is believed to orient the carboxylate group of Asp375 through the bridging water molecule Wat596.[7] Hydrogen bonding of His235 to Wat596 appears to enhance the hydrogen bonding of Wat596 to Asp375. The reaction models also show that the hydroxyl group of Ser244, but not the backbone NH, acts as an essential hydrogen-bond donor to His274, in agreement with the observation that Ser244 is a conserved residue in citrate synthase. Ser244 appears to indirectly stabilize the forming enolate by increasing the acidity and thus the hydrogen-bond donor ability of His274. Though Wat584, Wat585, Wat586, and Wat596 are not directly involved

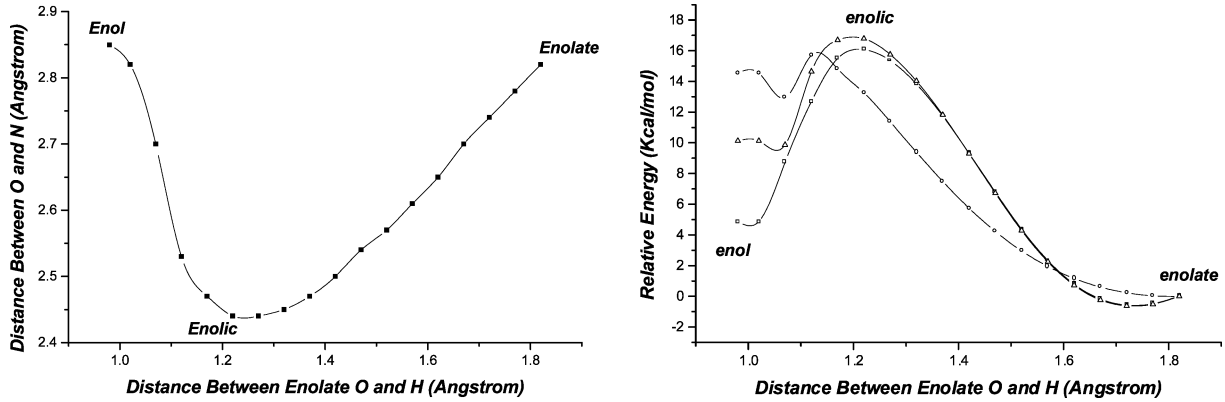

Figure 7. Locating possible intermediates in the citrate synthase catalyzed deprotonation of acetyl-CoA by monitoring N to O proton transfer. The distance between the thioacetate carbonyl oxygen and the His274 proton is taken as the reaction coordinate. The left panel shows the change of distance between the thioacetate carbonyl oxygen and the His274 nitrogen over the course of proton transfer. The right panel shows the variation of energy (without zero-point energy correction) over the course of proton transfer. Symbols represent the following: (○) HF/6-31+G* energy for the small model only; (△) ONIOM(HF/6-31+G*, PM3) energy for the medium-size model; (□) PM3 energy for the medium-size model.

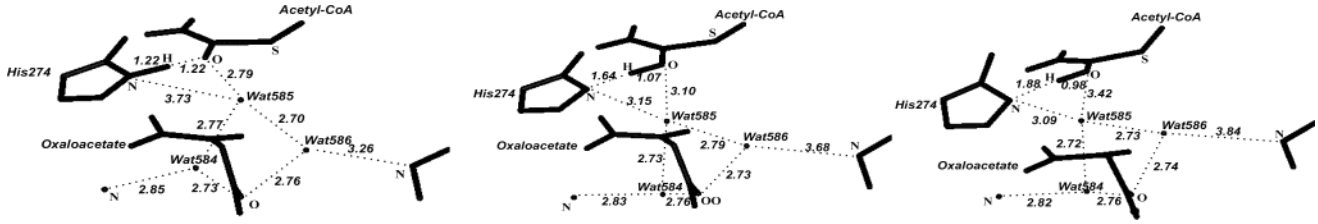

Figure 8. Important structures located on the proton-transfer pathway: (left) the enolic intermediate complex with an apparent low-barrier hydrogen bond; (middle) the structure with Wat585 forming hydrogen bonds to both acetyl-CoA and His274; (right) the enol complex with Wat585 forming a hydrogen bond with His274.

in the reaction center, they form secondary interactions through hydrogen bonding and apparently play important roles in balancing the activation energy. This cooperativity effect has also been observed in other enzymes.[37,38] Quantum mechanical treatment of the enzyme environment may be important for describing these subtle effects.

Comparison of Enolate, Enolic, and Enol Intermediates. While the calculated energy barrier for formation of the enolate reproduces the experimental result very well, further studies were done to compare the enolate with the enol and a half-protonated low-barrier hydrogen-bonded enolic intermediate to verify that the enolate is the true intermediate. Similar comparisons have previously supported an enolate intermediate.[9] To generate the enolic and enol structures, a pseudo-proton-transfer process was modeled by transferring the proton from His274 to the enolate oxygen, taking the distance between the enolate oxygen and the His274 proton as the reaction coordinate. Because of a charge assignment problem in the original MOPAC code, nitrogen cannot be assigned a negative charge so that MOZYME cannot be used in this case. The intermediate model was thus used, PM3 used as the lower level in ONIOM calculations. Figure 7 shows the change in distance between the enolate oxygen and His274 nitrogen over the course of proton transfer. Indeed, the O−N distance becomes less as the proton approaches the midway point between oxygen and nitrogen, in keeping with the short, strong or low-barrier hydrogen-bond proposal. However, the point that fits the low-barrier hydrogen-bond definition corresponds to an energy maximum in the energy profile at the level of ONIOM (HF/6-31+G*, PM3), indicating that the low-barrier hydrogen-bonded enolic intermediate is not a real intermediate in this system. Wat585 changes its hydrogen-bonding partner from the enolate oxygen to His274 upon conversion of the enolate to the enol (Figure 8). The shallow local minimum (Figure 7, right) corresponds to the enol complex in which Wat585 forms a hydrogen bond with both partners. The newly generated enol intermediate has only modest energy and structural differences from the structure used for generating the adiabatic pathway and thus is believed to belong within the same energy well. The enolic structure determined in this study is similar to that from the previous QM/MM study, having a His274 to enol(ate) N−O distance of 2.44 vs 2.48 Å in the QM/MM study.[7] The local minimum was used for subsequent energy calculations. The enol structure is also consistent with the QM-FE study, especially in that negatively charged His274 forms a hydrogen bond with Wat585.[10]

For further analysis, an expanded intermediate model with 232 atoms including additional functionality of the active-site environment was developed. The structures of the enolate, enolic, and enol complexes of the small-model component of the initial model were put into this expanded model and frozen during restrained geometry optimization of the remaining part of the model. The original and expanded models of the enolate, enolic, and enol intermediates were almost exactly superimposed, and the energy differences generated from the two models were almost identical. This indicates that this pseudo-proton transfer is a local process that has little effect on the surrounding protein environment.

Figure 9 shows the energy differences between enolate, enolic, and enol intermediates, taking the enolate as the energy standard. MP2 and B3LYP calculations both indicate that the enolic and enol intermediates have similar energies, both being higher in energy than the enolate by about 10−13 kcal/mol. This is fairly consistent with QM/MM studies, which predict only a slightly higher energy for the enol relative to the enolic intermediate.[9] The 12.4 kcal/mol energy difference between enol and enolate is smaller than the energy differences predicted in QM-FE (14.6 kcal/mol) and QM/MM (17.9 kcal/mol) studies.[9,10] The ONIOM−MOZYME method may allow the negatively charged histidine of the enol complex to be better stabilized by

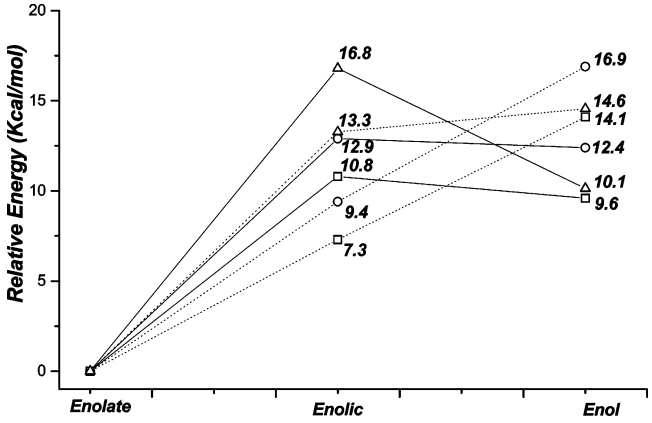

Figure 9. The energy differences among the three proposed intermediates (with the energy of the enolate as the standard): (△) HF/6-31+G*; (□) MP2/6-31+G*; (○) B3LYP/6-31+G*; (dotted line) small model only (with zero-point energy correction at HF/6-31+G*); (solid line) large model calculated using ONIOM.

TABLE 2: Energy Difference (with Zero-Point Energy Correction) for Formation of the Z vs E Enolates of Fluoroacetyl-CoA Calculated Using B3LYP/6-31+G* (Small Model) or ONIOM(B3LYP/6-31+G*, MOZYME(PM3)) (Large Model)

system	ΔE(Z−E) TS (kcal/mol)	ΔE(Z−E) enolate (kcal/mol)	exptl (kcal/mol)
small model	3.2	2.6	
large model	3.7	0.3	> 3.0

charge transfer and cooperativity effects of the hydrogen-bonding network,[39] thus resulting in a somewhat lower energy for the enol intermediate. Figure 9 illustrates this stabilization of the enol complex of the small model by the enzyme environment. The much greater stability of the enolate relative to the enol and enolic intermediates predicted by all three methods confirms that the enolate must be the true intermediate in the deprotonation reaction.

Deprotonation of Fluoroacetyl-CoA. This and previous computational studies indicate that the enolate is the true intermediate in the reaction of citrate synthase. However, this contradicts the conclusion based on the stereoselectivity observed in the deprotonation of fluoroacetyl-CoA by citrate synthase,[11,12] which has been attributed to formation of the more stable E enol.[15,16] The relative energies of the Z and E enolates and the transition states for their formation in the citrate synthase active site were thus evaluated (Table 2). In viewing the optimized enolate and transition-state complex structures, a repulsive interaction between the fluorine atom of the Z isomer and the carboxylate group of Asp375 appears to be a major influence. As shown in Figure 10, the fluoroacetyl group moves in opposite directions for the E and Z isomers in forming the transition state and intermediate, apparently to minimize the interaction of fluorine with Asp375. The resulting changes in structure disrupt the hydrogen bond with His274 to the extent that in the transition state His274 becomes hydrogen-bonded to Wat585 instead of the oxygen of the developing enolate. This apparent repulsive interaction between fluorine and Asp375 in the Z isomer and resulting changes in structure of the active site, in addition to the inherently greater stability of the E enolate, appears to be responsible for the 2.6 kcal/mol greater stability of the E enolate when only the energy of the small model is considered. A slightly larger difference of 3.2 kcal/mol is observed in the transition state for enolate formation. When the energy of the entire large model is considered, the E vs Z energy difference in the transition state becomes slightly greater while the energy difference in the enolate complex becomes very small. The latter appears to result from a favorable interaction between fluorine and Arg329 in the Z enolate and an unfavorable interaction between fluorine and oxaloacetate in the E enolate complex. These interactions appear to compensate for the energy difference in the small model. The Z and E enolates do not interact directly with Arg329 and oxaloacetate as observed in Figure 10, yet these charged groups appear to have significant effect on the relative stabilities of the Z and E enolates. This may be rationalized by the slow decay with distance of electrostatic interactions in the low dielectric constant environment of an enzyme active site. The large difference in activation energy for formation of the Z vs E enolates demonstrates that an enolate intermediate can adequately explain the stereoselectivity in the deprotonation of fluoroacetyl-CoA if deprotonation is rate-limiting. It appears that all computational methods are thus now in agreement in supporting an enolate intermediate for citrate synthase.

In prior computational studies of citrate synthase, the deprotonation step has been assumed to be the rate-limiting step. There is apparently no clear experimental evidence for this, because the very modest kinetic isotope effect ($k_H/k_D = 1.8$) with deteurium-labeled acetyl-CoA is inconclusive.[31] The present computational studies on the deprotonation of fluoroacetyl-CoA and their comparison with experimental results provide further support for the deprotonation step being the slow step in the overall reaction of citrate synthase. If the condensation step were rate-limiting, a high degree of stereoselectivity in this condensation of equilibrated Z and E enolates would appear unlikely. As shown in deletion component analysis, interaction with oxaloacetate has a large destabilizing effect on the enolate, which is balanced by other favorable interactions in the enolate complex. Because oxaloacetate is close to the enolate in the complex, the activation energy for bringing oxaloacetate and

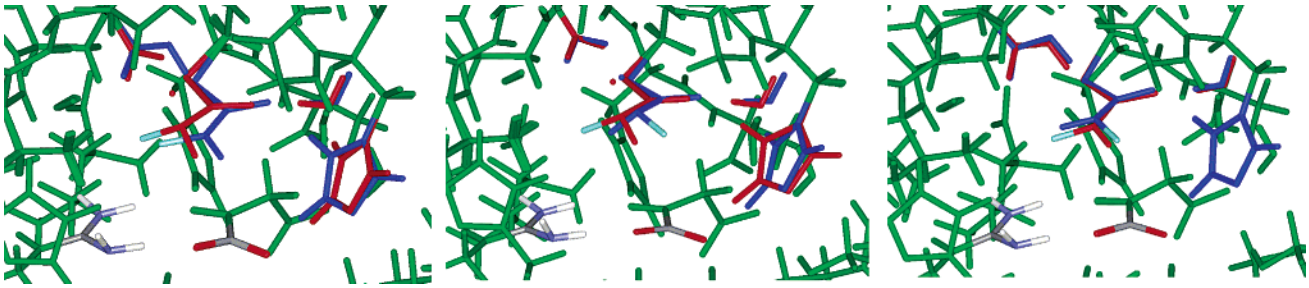

Figure 10. Overlayed transition state and intermediate structures for the Z and E isomers of fluoroacetyl-CoA (parts of Arg329 and oxaloacetate colored according to atom types): (left) superimposed transition state (red) and intermediate (blue) for the Z isomer; (middle) superimposed transition state structures of the Z (red) and E (blue) isomers; (right) superimposed intermediate structures of the Z (red) and E (blue) isomers.

the enolate close together in the condensation step is prepaid in the deprotonation step (about 7.2 kcal/mol). This further supports the expectation that the condensation step should be rapid and the deprotonation step rate-limiting.

Advantages and Limitations of the ONIOM−MOZYME Methodology. The ONIOM−MOZYME method described here extends quantum mechanical methods previously used in small molecule reactions to the description of an enzyme-catalyzed reaction. This method provides advantages over previous quantum mechanical model approaches by incorporating more of the enzyme environment into the model. For localized reactions such as the proton-transfer reaction studied in this work, a fairly small number of amino acid residues are directly involved in the reaction. The reaction may thus be adequately described by the ONIOM−MOZYME method in which the accuracy of high-level quantum calculations as used in studies of small molecule reactions are combined with full quantum treatment of a relatively large model system. The calculations reported here provide an excellent reproduction of the experimentally determined activation energy for citrate synthase and are in relatively good agreement with results from QM/MM studies.[9] This method also permits quantum mechanical treatment of more distant interactions as demonstrated in analysis of the citrate synthase catalyzed reaction of fluoroacetyl-CoA.

One limitation of this method, like other model-based methods, is that only a simplified model of the enzyme is studied and no dynamic effects are considered. Indeed, for reaction pathway generation, only the medium-size models were used with PM3, rather than MOZYME, as the lower level. The accuracy may also be limited by the level of theory that can be employed for the small model, as in this study geometries were generated using Hartree−Fock calculations, which may not provide an accurate treatment of proton transfer and hydrogen bonds. Furthermore, polarization of the small model environment by the larger model is only included at the lower level of theory. The semiempirical methods used for the larger models may also give poor treatment of protein structure. However, MOZYME and PM3 have been shown to give similar results in calculations on a small protein and gave structures that better matched a crystal structure than molecular mechanics, despite the tendency of PM3 to pyramidalize amide nitrogen.[23] Even though Arg329 plays some role in differentiating the relative stability of the E and Z enolates of fluoroacetyl-CoA, as discussed in the last section, the interaction between Arg329 and the enolate is not a direct hydrogen bond but only an electrostatic interaction, and so some pyramidalization of guanidine nitrogen will have little influence on the final result.

Conclusions

A new method for quantum mechanical treatment of a relatively large model of an enzyme was developed that combines ONIOM with the linearly scaling semiempirical method MOZYME. This method was demonstrated in a study of the citrate synthase catalyzed deprotonation of acetyl-CoA and fluoroacetyl-CoA. The calculations accurately reproduced the experimental activation energy for formation of the enolate intermediate. Energy differences among possible enolate, half-protonated enolic, and enol intermediates further confirmed that the enolate is the true intermediate and a half-protonated enolic species cannot exist as an intermediate in this reaction.

The study also showed that the stereoselectivity in deprotonation of fluoroacetyl-CoA by citrate synthase can be explained by an enolate intermediate. The calculated difference in activation energies for formation of the Z and E enolates accurately reproduced the experimentally observed stereoselectivity in this reaction. The results are consistent with the deprotonation step being the rate-determining step in the reaction of citrate synthase.

Acknowledgment. This work was supported by National Institutes of Health Grant GM45831.

Supporting Information Available: Complete descriptions of the geometries of all stationary points and the absolute energies for each. This material is available free of charge via the Internet at http://pubs.acs.org.

References and Notes

(1) Kluger, R. *Chem. Rev.* **1990**, *90*, 1151−1169.
(2) Gerlt, J. A.; Kozarich, J. W. *J. Am. Chem. Soc.* **1991**, *113*, 9667−9669.
(3) Remington, S. J. *Curr. Opin. Struct. Biol.* **1992**, *2*, 730−735.
(4) Guthrie, J. P.; Kluger, R. *J. Am. Chem. Soc.* **1993**, *115*, 11569−11572.
(5) Alagona, G.; Ghio, C.; Kollman, P. A. *J. Am. Chem. Soc.* **1995**, *117*, 9855−9862.
(6) Mulholland, A. J.; Richards, W. G. *J. Phys. Chem. B* **1998**, *102*, 6635−6646.
(7) Mulholland, A. J.; Richards, W. G. *Proteins: Struct., Funct., Genet.* **1997**, *27*, 9−25.
(8) Early work is reviewed in Mulholland, A. J.; Richards, W. G. In *Transition State Modeling for Catalysis*; Truhlar, D. G., Morokuma, K., Eds.; ACS Symposium Series 721, American Chemical Society: Washington, DC, 1999; p 467−505.
(9) Mulholland, A. J.; Lyne, P. D.; Karplus, M. *J. Am. Chem. Soc.* **2000**, *122*, 534−535.
(10) Donini, O.; Darden, T.; Kollman, P. A. *J. Am. Chem. Soc.* **2000**, *122*, 12270−12280.
(11) Carrell, H.; Glusker, J.; Villafranca, J.; Mildvan, A.; Dummel, R.; Kun, E. *Science* **1970**, *170*, 1412−1414.
(12) Walsh, C. *Adv. Enzymol.* **1982**, *55*, 197−289.
(13) Usher, K. C.; Remington, S. J.; Martin, D. P.; Drueckhammer, D. G. *Biochemistry* **1994**, *33*, 7753−7759.
(14) Schwartz, B.; Drueckhammer, D. G.; Usher, K. C.; Remington, S. J. *Biochemistry* **1995**, *34*, 15459−15466.
(15) O'Hagan, D.; Rzepa, H. S. *J. Chem. Soc., Chem. Commun.* **1994**, 2029−2030.
(16) O'Hagen, D.; Rzepa, H. S. *Chem. Commun.* **1997**, 645−652.
(17) Kahn, K.; Bruice, T. C. *J. Am. Chem. Soc.* **2000**, *122*, 46−51.
(18) Tvaroska, I.; Andre, I.; Carver, J. P. *J. Am. Chem. Soc.* **2000**, *122*, 8762−8776.
(19) Bruice, T. C.; Kahn, K. *Curr. Opin. Chem. Biol.* **2000**, *4*, 540−544.
(20) Tantillo, D. J.; Chen. J.; Houk, K. N. *Curr. Opin. Chem. Biol.* **1998**, *2*, 743−750.
(21) Titmuss, S. J.; Cummins, P. L.; Bliznyuk, A. A.; Rendell, A. P.; Gready, J. E. *Chem. Phys. Lett.* **2000**, *320*, 169−176.
(22) Greatbanks, S. P.; Gready, J. E.; Limaye, A. C. *J. Comput. Chem.* **2000**, *21*, 788−811.
(23) Stewart, J. J. P. *J. Mol. Struct. (THEOCHEM)* **1997**, *401*, 195−205.
(24) Svensson, M.; Humbel, S.; Froese, R. D. J.; Matsubara, T.; Sieber, S.; Morokuma, K. *J. Phys. Chem.* **1996**, *100*, 19357−19363.
(25) Svensson, M.; Humbel, S.; Morokuma, K. *J. Chem. Phys.* **1996**, *105*, 3654−3661.
(26) Dapprich, S.; Komaromi, I.; Byun, K. S.; Morokuma, K.; Frisch, M. *THEOCHEM* **1999**, *462*, 1−21.
(27) Torrent, M.; Vreven, T.; Musaev, D. G.; Morokuma, K.; Farkas, O.; Schlegel, H. B. *J. Am. Chem. Soc.* **2002**, *124*, 192−193.
(28) Frisch, M. J.; Trucks, G. W.; Schlegel, H. B.; Scuseria, G. E.; Robb, M. A.; Cheeseman, J. R.; Zakrzewski, V. G.; Montgomery, J. A., Jr.; Stratmann, R. E.; Burant, J. C.; Dapprich, S.; Millam, J. M.; Daniels, A. D.; Kudin, K. N.; Strain, M. C.; Farkas, O.; Tomasi, J.; Barone, V.; Cossi, M.; Cammi, R.; Mennucci, B.; Pomelli, C.; Adamo, C.; Clifford, S.; Ochterski, J.; Petersson, G. A.; Ayala, P. Y.; Cui, Q.; Morokuma, K.; Malick, D. K.; Rabuck, A. D.; Raghavachari, K.; Foresman, J. B.; Cioslowski, J.; Ortiz, J. V.; Stefanov, B. B.; Liu, G.; Liashenko, A.; Piskorz, P.; Komaromi, I.; Gomperts, R.; Martin, R. L.; Fox, D. J.; Keith, T.; Al-Laham, M. A.; Peng, C. Y.; Nanayakkara, A.; Gonzalez, C.; Challacombe, M.; Gill, P. M. W.; Johnson, B. G.; Chen, W.; Wong, M. W.; Andres, J. L.; Head-Gordon,

M.; Replogle, E. S.; Pople, J. A. *Gaussian 98*, revision A.7; Gaussian, Inc.: Pittsburgh, PA, 1998.
(29) Stewart, J. J. P. *MOPAC 2000 Manual*; Fujitsu Ltd.: Tokyo, 1999.
(30) Cornell, W. D.; Cieplak, P.; Bayly, C. I.; Gould, I. R.; Merz, K. M.; Ferguson, D. M.; Spellmeyer, D. C.; Fox, T.; Caldwell, J. W.; Kollman, P. A. *J. Am. Chem. Soc.* **1995**, *117*, 5179−5197.
(31) Halgren, T. A. *J. Comput. Chem.* **1996**, *17*, 490−519.
(32) *Spartan User's Guide*, version 5.0; Wavefunction, Inc.: Irvine, CA, 1997.
(33) Bayly, C. I.; Cieplak, P.; Cornell, W. D.; Kollman, P. A. *J. Phys. Chem.* **1993**, *97*, 10269−10280.
(34) Frisch, M. J. *J. Comput. Chem.* **1996**, *17*, 49−56.
(35) Bach, R. D.; Thorpe, C.; Dmitrenko, O. *J. Phys. Chem. B* **2002**, *106*, 4325−4335.
(36) Lau, E. Y.; Bruice, T. C. *J. Am. Chem. Soc.* **1998**, *120*, 12387−12394.
(37) Choi, G.; Ha, N.-C.; Kim, M.-S.; Hong, B.-H.; Oh, B.-H.; Choi, K. Y. *Biochemistry* **2001**, *40*, 6828−6835.
(38) Kim, D.-H.; Jang, D. S.; Nam, G. H.; Choi, G.; Kim, J.-S.; Ha, N.-C.; Kim, M.-S.; Oh, B.-H.; Choi, K. Y. *Biochemistry* **2000**, *39*, 4581−4589.
(39) Guo, H.; Salahub, D. R. *Angew. Chem., Int. Ed. Engl.* **1998**, *37*, 2985−2990.
(40) Lenz, H.; Eggerer, H. *Eur. J. Biochem.* **1976**, *65*, 237−246.